CHINESE OPTICS LETTERS

Vol. 19, No. 11 | November 2021

Frequency-modulated continuous-wave dual-frequency LIDAR based on a monolithic integrated two-section DFB laser

Changsheng Wang (王昌盛)[1], Yunshan Zhang (张云山)[2*], Jilin Zheng (郑吉林)[3**], Jin Li (李 晋)[3], Zhenxing Sun (孙振兴)[1], Jianqin Shi (施建琴)[1], Lianyan Li (李连艳)[2], Rulei Xiao (肖如磊)[1], Tao Fang (方 涛)[3], and Xiangfei Chen (陈向飞)[1]

[1] College of Engineering and Applied Sciences, Nanjing University, Nanjing 210093, China

[2] School of Optoelectronic Engineering, Nanjing University of Posts and Telecommunications, Nanjing 210023, China

[3] Photonics Information Technology Laboratory, Institute of Communication Engineering, Army Engineering University of PLA, Nanjing 210007, China

*Corresponding author: yszhang@njupt.edu.cn

**Corresponding author: zhengjilinjs@126.com

Received February 8, 2021 | Accepted April 27, 2021 | Posted Online September 1, 2021

We demonstrate a high-resolution frequency-modulated continuous-wave dual-frequency LIDAR system based on a monolithic integrated two-section (TS) distributed feedback (DFB) laser. In order to achieve phase locking of the two lasers in the TS-DFB laser, the sideband optical injection locking technique is employed. A high-quality linear frequency-modulated signal is achieved from the TS-DFB laser. Utilizing the proposed LIDAR system, the distance and velocity of a target can be measured accurately. The maximum relative errors of distance and velocity measurement are 1.6% and 3.18%, respectively.

Keywords: dual-frequency LIDAR; integrated two-section DFB laser; frequency-modulated continuous wave; linear frequency modulation.

DOI: 10.3788/COL202119.111402

1. Introduction

High-resolution LIDAR has important applications in scientific research, industrial production, and unmanned driving[1–4]. There are two common detection methods of conventional LIDAR, namely, the time of flight (TOF) method and frequency-modulated continuous-wave (FMCW) method[5,6]. Although TOF LIDAR has a relatively simple system structure, it cannot measure a target in short distance due to its blind spot. The spatial resolution of TOF LIDAR is determined by the pulse width and the precision of the timer. Consequently, high-quality pulse sources with pulse width of a few nanoseconds and high-precision timers are required in TOF LIDAR systems[7]. Besides, TOF LIDAR is commonly used to detect the distance of a target, and it is difficult to achieve accurate velocity measurement simultaneously, such as three-dimensional (3D) coherent LIDAR[5,8]. The FMCW LIDAR can directly measure the distance and velocity of a moving target simultaneously and does not need fast electrical instruments. Further, heterodyne detection technology is utilized in the FMCW LIDAR, which can avoid external interference from environment or other LIDARs. However, the FMCW LIDAR is highly sensitive to atmospheric turbulence and the speckle noise induced by the target's roughness, which results in lower measurement accuracy. Besides, the measurement accuracy of distance and velocity also depends on the linewidth and modulation linearity of the light source. Consequently, a high-quality linear frequency-modulated (LFM) laser with narrow linewidth is essential to the FMCW LIDAR, which is a very challenging task and leads to the high cost of LIDAR production[9,10].

Dual-frequency (DF) LIDAR can effectively weaken the influence of atmospheric turbulence and speckle noise. It can also reduce the difficulty of signal processing compared with the common single-frequency LIDAR[3,11–13]. However, the conventional DF LIDAR is constituted of multiple separate devices, which is complicated and impractical[12]. Moreover, the DF LIDAR is mainly used to measure the velocity of a target, and it cannot achieve the distance information[3].

In this article, an FMCW-DF LIDAR is demonstrated experimentally based on a monolithic integrated two-section (TS) distributed feedback (DFB) laser. The proposed LIDAR can measure the distance and velocity of a target simultaneously. According to the measured results, the maximum relative errors (REs) of the distance and velocity are 1.6% and 3.18%, respectively.

2. Characteristics of the Two-Section DFB Laser

Figure 1 shows the schematic of the monolithic integrated TS-DFB laser utilized in the proposed LIDAR. It consists of two in-series DFB lasers including the master laser (ML) and the slave laser (SL). The cavity lengths of the TSs L_m and L_s both are 650 μm. The epitaxy of the device is grown by conventional two-stage metal organic chemical vapor deposition (MOCVD) on an n-InP substrate. An n-InP buffer layer, an n-InAlGaAs lower optical confinement layer, an InAlGaAs multiple-quantum-well structure, a p-InGaAsP upper optical confinement layer, and a p-InGaAsP grating layer are successively grown on an n-InP substrate in the first epitaxial growth. Both gratings in the TSs are designed by the reconstruction-equivalent-chirp (REC) technique with an identical seed grating period $\Lambda_0 = 256$ nm, the REC technique was used to simplify the fabrication of the gratings of DFB lasers or laser arrays and enhance the precision of the grating[14]. A conventional holographic exposure combined with conventional photolithography is used to form the sampled gratings. After the fabrication of the sampled grating, a p–InP cladding layer and a contact layer are successively regrown over the entire structure in the second epitaxial growth. Then, a conventional ridge waveguide p–InGaAs processing is performed, and p-metal contact windows are opened for metallization. The ML and SL are electrically isolated with each other, and their bias currents are labeled as I_m and I_s. Finally, both facets of the devices are coated by anti-reflection (AR) coatings with reflectivity less than 1% to suppress the Fabry–Perot modes of the lasers[15].

Through tuning the sampling periods P_m and P_s, the lasing wavelengths of the TSs and detuning frequency can be controlled accurately with deviations less than 0.2 nm[16,17], which is sufficient for the generation of two modes. Further, by changing the bias current of ML and SL, we can obtain the required wavelength difference between the two lasers (i.e., the frequency of the beat signal generated by the optical heterodyne).

Figure 2 shows the experimental setup for investigating the performance of the TS-DFB laser. The ML and SL are biased with constant direct current (DC), and the SL is also modulated by a radio frequency (RF) signal generated by an arbitrary waveform generator (AWG). The light from the laser is spilt into two beams by an optical coupler (OC). One beam is injected into a high-speed photodetector (PD) to observe the performance of the beat signal. The optical spectrum analyzer (OSA) is used to monitor the optical spectrum simultaneously. Figure 3(a) shows the optical spectra of the TS-DFB laser without RF modulation signal when the bias currents (I_m, I_s) of the ML and SL are 70 mA and 50 mA, respectively. The ML and SL can operate independently with wavelengths of $\lambda_{ML} = 1549.44$ nm and $\lambda_{SL} = 1549.56$ nm, respectively, i.e., the frequency difference of the two lasers is about $\Delta f = 15$ GHz. Figure 3(b) shows the optical spectrum when the SL is modulated by a 7.5 GHz RF signal, the power of which remains 10 dBm in our experiment. It can be seen that several symmetric sidebands are generated on both sides of the SL frequency, and the frequency of the +2nd sideband is equal to the ML frequency. Due to the sideband injection locking technique, the phases of the ML and SL are locked[18]. When the light from the laser is directed into the PD, a 15 GHz beat signal is generated. As shown in Fig. 4, when the

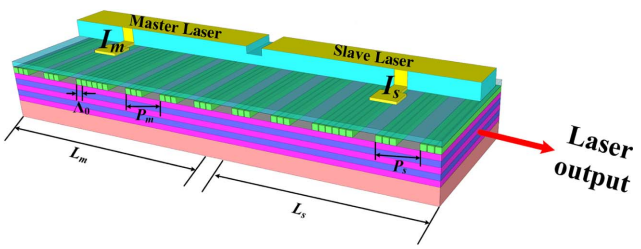

Fig. 1. Schematic of the TS-DFB laser.

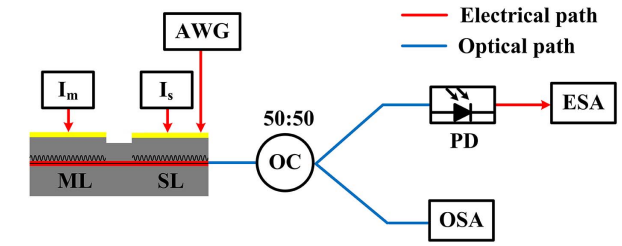

Fig. 2. Experimental setup for laser characteristic measurement. AWG, arbitrary waveform generator; OC, optical coupler; PD, photodetector; ESA, electrical spectrum analyzer; OSA, optical spectrum analyzer.

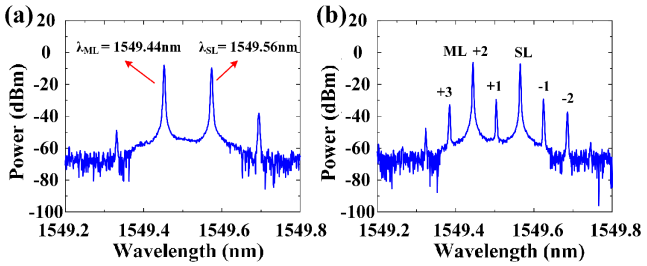

Fig. 3. (a) Optical spectrum of the TS-DFB laser when I_s = 50 mA and I_m = 70 mA; (b) optical spectrum when a 7.5 GHz RF signal is applied to the SL.

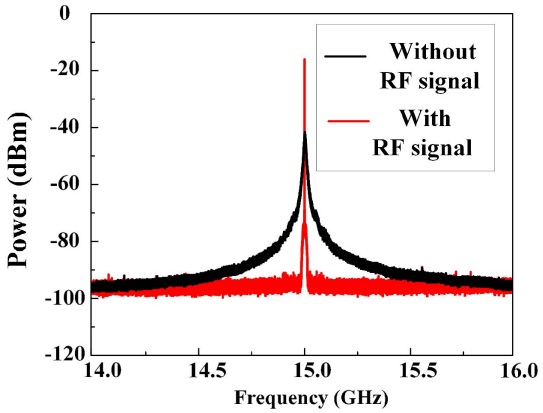

Fig. 4. Spectra of beat signals for the case of SL with and without RF signal modulation.

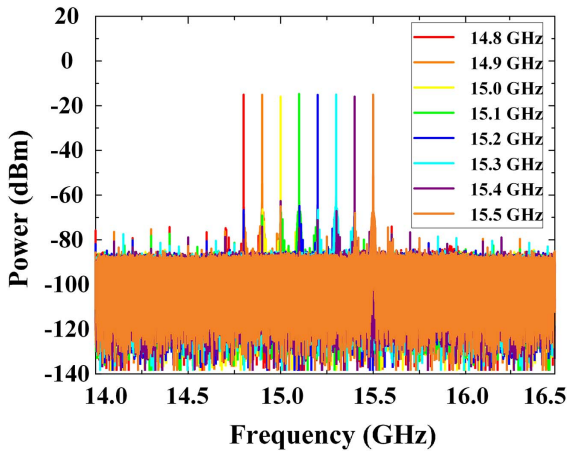

Fig. 5. Spectra of the beat signal with the different RF signals.

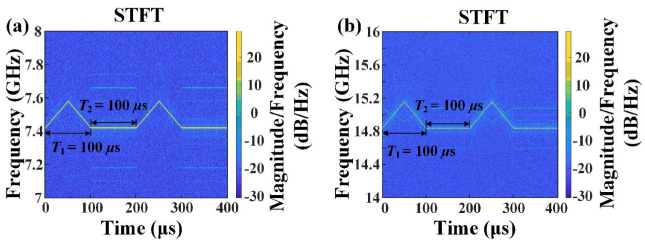

Fig. 6. Time-frequency curve of (a) the RF signal and (b) the beat signal.

SL is modulated by the RF signal, the beat signal is improved significantly, which is very beneficial to the accuracy of distance and velocity measurement.

It is found that the ML frequency varies with the frequency of the +2nd-order modulation sideband in the injection locked state, i.e., the frequency of the beat signal changes with the RF signal. Figure 5 shows the spectra of the beat signal, which varies from 14.8 GHz to 15.5 GHz when the RF signal frequency changes from 7.4 GHz to 7.75 GHz. Hence, if the RF signal is an LFM signal, the beat signal is also an LFM signal with high quality. Figures 6(a) and 6(b) show the time-frequency diagrams of the RF signal and the beat signal. It is obvious that the RF signal is an LFM signal with frequency chirped from 7.42 GHz to 7.58 GHz. The RF signal consists of an up–down ramp segment and a constant frequency segment. The lengths of the two segments (T_1 and T_2) are both 100 μs. The beat signal is also an LFM signal, and its frequency changes from 14.84 GHz to 15.16 GHz with the same period as the RF signal. Using the sideband injection locking technique, the center frequency and the modulation band of the beat signal are doubled compared with the RF signal.

3. Experimental Setup and Theory Principle

Figure 7 shows experiment setup of the proposed FMCW-DF LIDAR. The LFM DF TS-DFB laser discussed above is utilized. The SL is modulated by the LFM RF signal shown in Fig. 6(a). The light from the laser is split into two beams by a 50:50

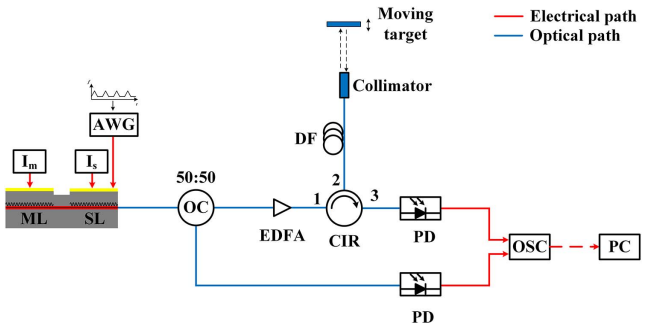

Fig. 7. Experimental setup for the proposed system. AWG, arbitrary waveform generator; OC, optical coupler; EDFA, erbium-doped fiber amplifier; CIR, circulator; DF, delay fiber; PD, photodetector; OSC, oscilloscope; PC, computer.

OC. The first beam is directed into a high-speed photodetector (PD2) as the reference signal. The second beam is amplified by an erbium-doped fiber amplifier (EDFA), sent to port-1 of a circulator, and then transmitted through a delay fiber and collimator in port-2 to the moving target. The back-reflected light from the target with Doppler shift is coupled to the circulator by the same delay fiber and collimator. It should be noted that the moving target is a mirror on a motorized translation stage, the target velocity is controlled by the translation stage, and target distance here is defined by the length of the delay fiber, so we can replace the distance of the target in space by using delayed fiber of different lengths. The back-reflected light is injected to another high-speed photodetector (PD1) through port-3 of the circulator. The electrical signals from PD1 and PD2 are acquired by a real-time oscilloscope (OSC). Then, the signals are digital frequency mixed and analyzed by a computer.

Figure 8 shows the schematic of the time-frequency domain diagrams of the reference beat signal, back-reflected beat signal, and mixing signal of the two signals. The frequency of the reference beat signal can be expressed as

$$f_T(t) = \begin{cases} f_1 + kt, & t \in [0, t_1/2] \\ f_2 - kt, & t \in [t_1/2, t_1], \\ f_1, & t \in [t_1, t_2] \end{cases} \tag{1}$$

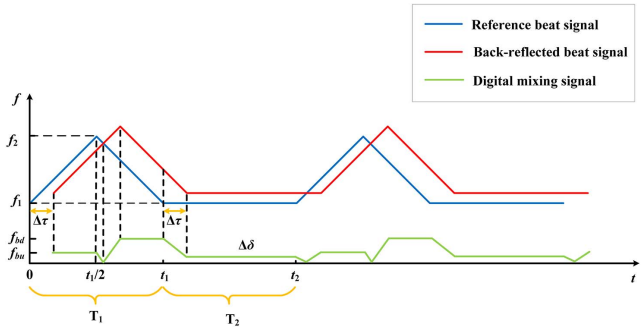

Fig. 8. Schematics of the time-frequency diagrams of the reference beat signal (blue line), back-reflected beat signal (red line), and the mixing signal (green line).

where f_1 and f_2 are the initial frequencies of the up-chirped and down-chirped segments, respectively, k is the chirp rate $k = 2(f_2 - f_1)/T_1 = 2B/T_1$, and B is the modulation band of the reference beat signal. The frequency of the back-reflected signal is expressed as

$$f_R(t) = \begin{cases} f_1 + k(t-\tau) + (\delta_m - \delta_s), & t \in [0, t_1/2] \\ f_2 - k(t-\tau) + (\delta_m - \delta_s), & t \in [t_1/2, t_1] \\ f_1 + (\delta_m - \delta_s), & t \in [t_1, t_2] \end{cases}. \quad (2)$$

Here, τ is the transmission delay of the back-reflected signal compared with the reference light. The Doppler shifts δ_m and δ_s depend on the target velocity as $\delta_m = 2v_t f_m/c$ and $\delta_s = 2v_t f_s/c$, where v_t is the target velocity, f_m is the frequency of the ML, f_s is the frequency of the SL, and c is the speed of light. Since $f_m > f_s$, $\delta_m > \delta_s$.

After frequency mixing and lowpass filtering, three low-frequency components can be obtained from the mixing signal, which is shown in Eq. (3):

$$\begin{cases} f_{bu} = k\tau - (\delta_m - \delta_s) \\ f_{bd} = k\tau + (\delta_m - \delta_s) \\ \Delta\delta = \delta_m - \delta_s \end{cases}. \quad (3)$$

The distance and velocity of the moving target can be simultaneously derived as

$$\begin{cases} R = \frac{c\tau}{2n} = \frac{cT_1(f_{bu}+f_{bd})}{8nB} = \frac{cT_1\Delta f_b}{4nB} \\ v_t = \frac{c\Delta\delta}{2\Delta f} \end{cases}, \quad (4)$$

where $\Delta f_b = (f_{bu} + f_{bd})/2$, $\Delta f = f_m - f_s = c(1/\lambda_m - 1/\lambda_s)$, and n is the optical fiber refractive index. It should be noted that because the maximum target velocity in this experiment is less than 2 m/s, the Doppler shift difference $\Delta\delta$ is only a few tens of hertz. Consequently, $\Delta\delta$ is far less than f_{bu} and f_{bd} (i.e., f_{bu} is approximately equal to f_{bd}). Since $\Delta\delta$ is so small, it is difficult to measure $\Delta\delta$ accurately in the up–down ramp segment of the signal, and the constant frequency segment is employed for the velocity measurement.

4. Experimental Results

Figure 9 shows the measured time-frequency diagrams of the reference beat signal, back-reflected beat signal, and digital mixing signal when the distance and velocity are set at 2935 m and 0.51 m/s, respectively. It can be seen that the Doppler shift difference $\Delta\delta$ is close to zero frequency, and f_{bu} is approximately equal to f_{bd}.

To obtain more precise results, the fast Fourier transform (FFT) method is used to process the signals. Figure 10 presents the spectra of the digital mixing signals for the measurements of distance and velocity of the target. According to Eq. (4), the

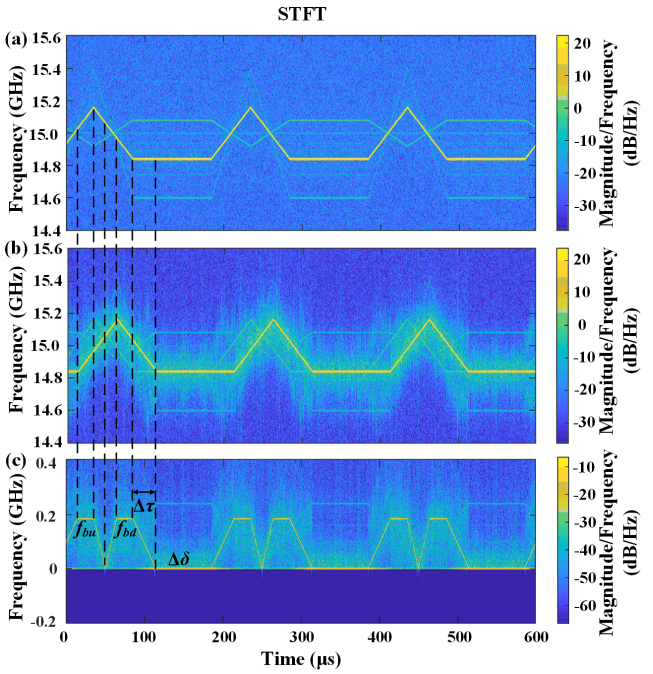

Fig. 9. Measured time-frequency diagrams of (a) the reference beat signal, (b) the back-reflected beat signal, and (c) the digital mixing signal.

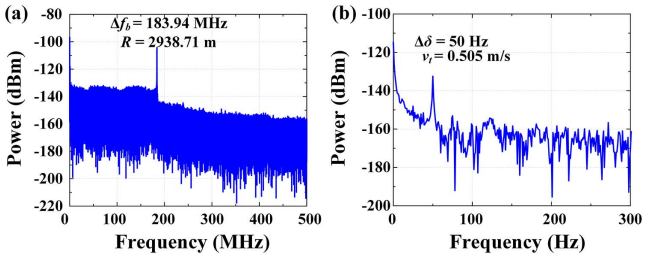

Fig. 10. Spectra of the digital mixing signals for (a) the distance measurement and (b) the velocity measurement.

measured distance and velocity are 2938.71 m and 0.505 m/s, which agree well with the set value.

To investigate the performance of the FMCW-DF LIDAR, targets with various distances and velocities are measured, and the measurement errors and REs are also demonstrated. Figure 11(a1) shows the distance and velocity measurement results when the distance is changed from 15 m to 2935 m with a fixed speed of 146.3 mm/s. Figures 11(a2) and 11(a3) show the distance and velocity measurement errors and REs at different target distances. The maximum distance measurement error is 4.63 m when the target distance is set at 1 km. The maximum velocity measurement error is 0.00132 m/s. The maximum REs of the distance and velocity measurements are 1.6% and 0.9%, respectively. Figure 11(b1) illustrates the distance and velocity measurement results when the speed of the target varies from 7.3 mm/s to 1462.5 mm/s with a fixed distance of 1115 m. In this case, the maximum distance error and velocity error are

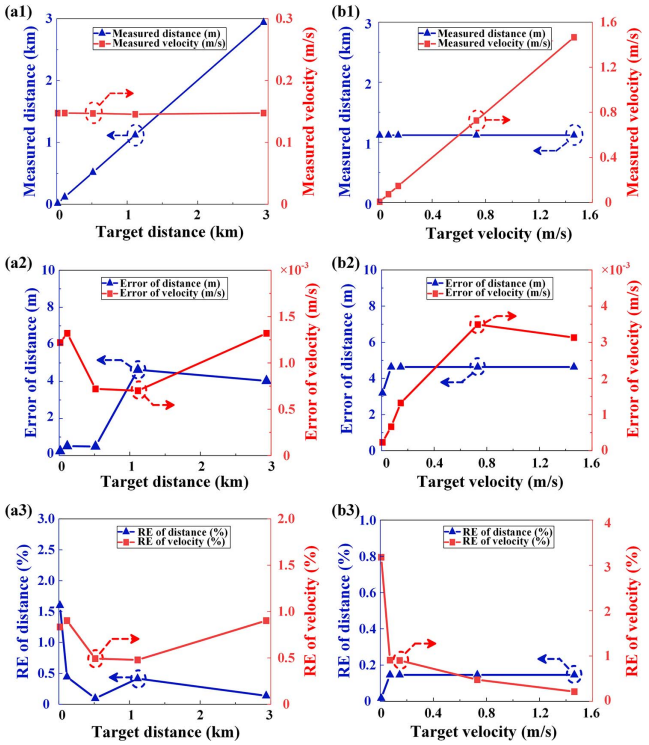

Fig. 11. Measurement results of the LIDAR. (a1)–(a3) Measured distances and velocities, measurement errors, and REs when target velocity is fixed at 146.3 mm/s with different distances. (b1)–(b3) Measured distances and velocities, measurement errors, and REs when target distance is fixed at 1115 m with various velocities.

4.63 m and 0.00349 m/s, respectively. The REs of the distance and velocity measurement are 0.14% and 3.18%.

5. Conclusion

An FMCW-DF LIDAR based on a monolithic integrated TS-DFB laser is experimentally demonstrated. Utilizing the sideband injection locking technique, the DF TS-DFB laser with high-quality LFM beat signal is realized, which is employed in the proposed LIDAR. The performance of the LIDAR is also experimentally investigated. The FMCW-DF LIDAR can accurately measure the distance and velocity of a target simultaneously. The maximum relative measurement errors of the distance and velocity are 1.6% and 3.18%, respectively.

Acknowledgement

This work was supported in part by the National Key R&D Program of China (No. 2018YFA0704402), National Natural Science Foundation of China (Nos. 61974165 and 61975075), National Natural Science Foundation of China for the Youth (No. 62004105), Science and Technology Project, and Natural Science Foundation of Jiangsu Province (No. BE2019101).

References

1. R. H. Couch, C. W. Rowland, K. S. Ellis, M. P. Blythe, C. R. Regan, M. R. Koch, C. W. Antill, Jr., W. L. Kitchen, J. W. Cox, J. F. DeLorme, S. K. Crockett, R. G. Remus, J. C. Casas, and W. H. Hunt, "Lidar in-space technology experiment (LITE): NASA's first in-space lidar system for atmospheric research," Opt. Eng. **30**, 88 (1991).
2. B. Schwarz, "Lidar: mapping the world in 3D," Nat. Photon. **4**, 429 (2010).
3. R. Diaz, S.-C. Chan, and J.-M. Liu, "Lidar detection using a dual-frequency source," Opt. Lett. **31**, 3600 (2006).
4. R. H. Rasshofer and K. Gresser, "Automotive radar and lidar systems for next generation driver assistance functions," Adv. Radio Sci. **3**, 205 (2005).
5. J. Lee, Y. J. Kim, K. Lee, S. Lee, and S. W. Kim, "Time-of-flight measurement with femtosecond light pulses," Nat. Photon. **4**, 716 (2010).
6. S. Guang and W. Wen, "Dual interferometry FMCW laser ranging for high precision absolute distance measurement system," Infrared Laser Eng. **45**, 806001 (2016).
7. Y. Li, Y. Cai, R. Li, H. Shi, H. Tian, M. He, Y. Song, and M. Hu, "Large-scale absolute distance measurement with dual free-running all-polarization-maintaining femtosecond fiber lasers," Chin. Opt. Lett. **17**, 091202 (2019).
8. Z. Lu, W. Lu, Y. Zhou, J. Sun, Q. Xu, and L. Wang, "Three-dimensional coherent ladar based on FMCW and its flight demonstration," Chin. Opt. Lett. **17**, 092801 (2019).
9. U. Sharma, G. Chen, J. U. Kang, I. Ilev, and R. W. Waynant, "Fiber optic confocal laser Doppler velocimeter using an all-fiber laser source for high resolution measurements," Opt. Express **13**, 6250 (2005).
10. C. H. Cheng, J. W. Lee, T. W. Lin, and F. Y. Lin, "Dual-frequency laser doppler velocimeter for speckle noise reduction," Opt. InfoBase Conf. Pap. **20**, 4914 (2012).
11. J. T. Dobler, B. M. Gentry, and J. A. Reagan, "Dual-frequency technique for Doppler wind lidar measurements," Proc. SPIE **4484**, 82 (2002).
12. H. Zhu, J. Chen, D. Guo, W. Xia, H. Hao, and M. Wang, "Birefringent dual-frequency laser Doppler velocimeter using a low-frequency lock-in amplifier technique for high-resolution measurements," Appl. Opt. **55**, 4423 (2016).
13. H. K. Sung, T. Jung, M. C. Wu, D. Tishinin, K. Y. Liou, and W. T. Tsang, "Optical generation of millimeter-waves using monolithic sideband injection locking of a two-section DFB laser," in *16th Annual Meeting of the IEEE Lasers and Electro-Optics Society* (2003), p. 1005.
14. Y. Shi, X. Chen, Y. Zhou, S. Li, L. Lu, R. Liu, and Y. Feng, "Experimental demonstration of eight-wavelength distributed feedback semiconductor laser array using equivalent phase shift," Opt. Lett. **37**, 3315 (2012).
15. Y. Zhang, L. Li, Y. Zhou, G. Zhao, Y. Shi, J. Zheng, Z. Zhang, Y. Liu, L. Zou, Y. Zhou, Y. Du, and X. Chen, "Modulation properties enhancement in a monolithic integrated two-section DFB laser utilizing side-mode injection locking method," Opt. Express **25**, 27595 (2017).
16. Y. Dai and X. Chen, "DFB semiconductor lasers based on reconstruction-equivalent-chirp technology," Opt. Express **15**, 2348 (2007).
17. J. Lu, S. Liu, Q. Tang, H. Xu, Y. Chen, and X. Chen, "Multi-wavelength distributed feedback laser array with very high wavelength-spacing precision," Opt. Lett. **40**, 5136 (2015).
18. J. M. Liu and T. B. Simpson, "Four-wave mixing and optical modulation in a semiconductor laser," IEEE J. Quantum Electron. **30**, 957 (1994).